Interference of parallel cylindrical Langmuir probes

J. R. Sanmartín[a)]
Escuela Técnica Superior de Ingenieros Aeronáuticos, Universidad Politécnica de Madrid, Madrid 28040, Spain

R. D. Estes
Harvard-Smithsonian Center for Astrophysics, 60 Garden St., Cambridge, Massachusetts 02138

(Received 15 March 2001; accepted 12 June 2001)

Current to a cylindrical probe of arbitrary cross section is discussed. Previous results for circular cylinders at the high bias and moderate radius R of interest for electrodynamic bare tethers, for which space charge may be ignored over a large neighborhood of the probe, depend in separate ways on both R and perimeter p. These results are extended to a general convex cross section by introducing certain equivalent radius R_{eq}. For any concave cross section, results use a proper equivalent perimeter p_{eq}, in addition to R_{eq}. Finally, for the joint cross section of separate parallel probes, certain effective perimeter p_{eff} replaces p_{eq}. Rules to determine R_{eq}, p_{eq}, and p_{eff} are used to discuss collection interference among two or more parallel cylinders when brought from far away to contact. © *2001 American Institute of Physics.* [DOI: 10.1063/1.1390332]

I. INTRODUCTION

A bare electrodynamic tether would efficiently collect electrons over part of its length, left uninsulated.[1] A theory of cylindrical Langmuir probes at high positive bias has been recently developed to analyze bare-tether collection,[2,3] which the experiment ProSEDS (Propulsive Small Expendable Deployer System) will test in orbit in June 2002.[4] Marshall Space Flight Center has proposed the use of bare tethers for continuous reboost of the International Space Station.[5] A point of interest is how two or more close, parallel tethers would interfere with each other in collecting. Such an arrangement may be motivated by tether survivality,[6] tether efficiency in high thrust propulsion,[7] or just tether current with limited length. Here we study tether interference by first extending previous results on collection to cross sections other than circles.

At positive bias, the electron current I to a cylindrical probe in an unmagnetized plasma, with electron distribution function isotropic at infinity, and no trapped-electron population, has an upper bound [the orbital-motion-limited (OML) current], which is reached if the probe cross section is both small and convex enough. The OML current density is uniform over the probe surface independently of its shape;[8] at the very high bias of interest for bare tethers, the current is very accurately given as

$$I_{\mathrm{OML}}(p)\approx(p/\pi)LeN_\infty\sqrt{2e\Phi_P/m_e}\propto p. \tag{1}$$

Here, L, Φ_P, and p are probe length, bias, and perimeter of its cross section, and N_∞ is the unperturbed electron density. We had discussed elsewhere magnetic and trapped-electron effects[2] and the anisotropy arising in the bare-tether case from its orbital velocity.[3]

As we shall see, current fails to reach the OML value if the cross section is either large or nonconvex, with either type of failure relating to a quite different feature in the potential field. We review results for circular cylinders in Sec. II and then consider separately the size effects for a general convex cross section (Sec. III), and effects of shape for cross sections that are concave (Sec. IV) or made of disjoint parts (Sec. V). We use results in discussing interference among two or more parallel probes in Sec. VI, showing how total current decreases as distances among them decrease. The fact that the potential obeys the Laplace equation over a large probe neighborhood proves essential for the determination of interference effects, which are resumed in Sec. VII.

II. REVIEW OF RESULTS FOR A CIRCULAR CYLINDER

Using high-bias approximations and the circular symmetry of this basic problem allowed solving Poisson's equation for the potential $\Phi(r)$, and determining the electron distribution function everywhere, in particular at the probe surface. Results from Ref. 2 for the current may then be written as

$$I=I_{\mathrm{OML}}(p) \quad \text{for } R<R_{\max}, \tag{2}$$

$$R=p/2\pi, \tag{3}$$

$$R_{\max}=\lambda_{\mathrm{De}}\times\text{a function of } e\Phi_P/kT_e,\quad T_i/T_e, \tag{4}$$

with λ_{De} the electron Debye length. The ratio $R_{\max}/\lambda_{\mathrm{De}}$, which was determined in Ref. 2, is about unity at conditions of interest for tethers, $T_i/T_e\sim1$, $e\Phi_P/kT_e\sim10^3$.

When R is taken larger than $R_{\max}$ (or when λ_{De}, and thus $R_{\max}$, decreases with growing density N_∞ at fixed R), the current drops below the OML value as a size effect related to behavior of the potential profile $\Phi(r)$ *far* from the probe. For $R\sim R_{\max}$ the profile at high bias exhibits a relative minimum of $r^2\Phi(r)$ at certain faraway radius,

a)Electronic mail: jrs@faia.upm.es

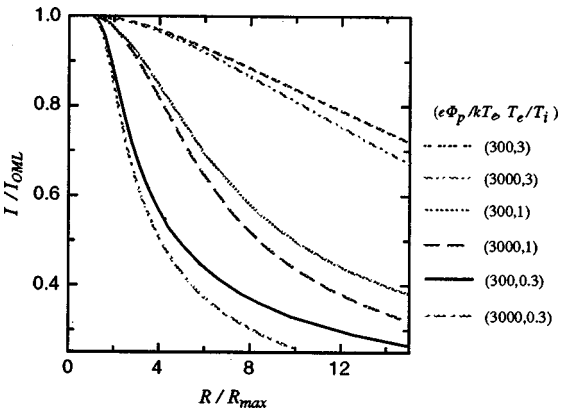

FIG. 1. Current ratio I/I_{OML} vs $R/R_{\max}$ for a few values of T_i/T_e and $e\Phi_P/kT_e$.

$$r_0 \sim R\sqrt{e\Phi_P/kT_e} \gg R; \tag{5}$$

for $R>R_{\max}$, that minimum of $r^2\Phi(r)$ lies below its value $R^2\Phi_P$ at the probe.[2] Then, trajectories that hit the probe within some range of glancing angles are *unpopulated*: the probe being attractive, they come, not from the background plasma, but from other points on the (nonemissive) probe, after having turned back at distances $\sim r_0$.

The current I beyond $R_{\max}$ may be written as

$$I = I_{\mathrm{OML}}(p) \times G\left[\frac{R}{\lambda_{\mathrm{De}}}, \frac{e\Phi_P}{kT_e}, \frac{T_i}{T_e}\right] \quad \text{for } R>R_{\max} \tag{2'}$$

with results for the function G given in Ref. 3. Equations (2) and (2′) determine the current in terms of probe radius and perimeter, which are related by (3). Using Eq. (4), the function G in (2′) can also be written in terms of $R/R_{\max}$, $e\Phi_P/kT_e$, and T_i/T_e, as shown in Fig. 1 for later use.[3]

An important additional result is that, because of the very high bias, the space charge has negligible effects within some extended region around the probe, where the Laplace equation holds even with $R \sim \lambda_{\mathrm{De}}$, and the potential $\Phi(r)$ takes the form[2,3]

$$\Phi/\Phi_P \approx 1 - \alpha \ln(r/R), \quad R \ll r \ll r_0, \tag{6}$$

$$1/\alpha \sim \ln(r_0/R) \sim \ln\sqrt{e\Phi_P/kT_e} \quad \text{(moderately large)}. \tag{7}$$

This will allow to extend the analysis to cylinders with arbitrary cross section. We note that, with other parameters fixed, α increased weakly with R (or p).

III. SIZE EFFECT FOR A GENERAL CONVEX CROSS SECTION

First consider elliptical cross sections, and use elliptical coordinates v, w, defined in terms of Cartesian coordinates in the cross section plane as

$$x = a\cos v \cosh w, \quad y = a \sin v \sinh w,$$

$$0 \leq v < 2\pi, \quad 0 \leq w < \infty,$$

with $w(x,y) = \text{const}$ representing confocal ellipses, which approach circles as w increases. Any value $w=w_P$ serves to describe an elliptical cross section of semiaxes $a\cosh w_P$ and $a\sinh w_P$, and eccentricity $1/\cosh w_P$. Because of the high bias, the Laplace equation is again valid within an extended probe vicinity, which reaches where w ellipses are near circles,

$$w \approx \ln(2r/a) \quad \text{for } w>w^* \quad (w^*=1.5, \text{ say}). \tag{8}$$

As in Ref. 2 for the limit case $w_P=0$, it may be shown that $\Phi(v,w)$ will be nearly independent of v everywhere, although the electric field will be nearly radial for $w>w^*$ only.

The simplified Laplace equation for the probe vicinity then yields

$$d^2\Phi/dw^2 \approx 0 \Rightarrow \Phi/\Phi_P \approx 1 - \alpha(w - w_P).$$

Within some limited w-range beyond w^* we have, using (8),

$$\Phi/\Phi_P \approx 1 - \alpha \ln(r/R_{\mathrm{eq}}), \tag{9}$$

$$R_{\mathrm{eq}} \equiv (a\cosh w_P + a \sinh w_P)/2, \tag{10}$$

to be compared with Eq. (6). From the perimeter for an ellipse we finally get

$$R_{\mathrm{eq}} = p \times (1 + \tanh w_P)/8E(m) \quad (m \equiv 1/\cosh^2 w_P); \tag{11}$$

here E is the complete elliptical integral of the second kind and m its parameter. Beyond w^*, the potential behaves as in the case of a circle of radius R_{eq}, the coefficient α being taken from the solution for a circle of that radius. Eccentricity values 1 [$E(1)=1$, $R_{\mathrm{eq}}=p/8$] and 0 [$E(0)=\pi/2$, $R_{\mathrm{eq}}=p/2\pi$], correspond to thin tapes and circles.[2]

For any other convex cross section, characterized by its perimeter p, one can also determine an equivalent radius $R_{\mathrm{eq}} \propto p$, to be used in Eqs. (2), (2'), (5), and (6). The OML law will stay valid with regard to the size as long as R_{eq} remains below $R_{\max}$, shape details being irrelevant to this size effect. The Laplace equation, valid near the probe, filters out to the far field all information on shape except for the equivalent radius R_{eq}.

Equation (9) for the elliptical cross section may be rewritten as

$$\frac{\Phi}{\Phi_P} = \frac{-\ln(r/r_\infty)}{\ln(r_\infty/R_{\mathrm{eq}})} = -\alpha \ln\frac{r}{r_\infty}, \tag{12}$$

where the radius r_∞ was defined by writing $\ln(r_\infty/R_{\mathrm{eq}}) \equiv 1/\alpha$, thus being comparable to r_0. To determine R_{eq} for a general case, one solves the Laplace equation between the contour of the given cross section, where $\Phi=\Phi_P$, and a circle of radius $r_\infty \gg p$, where $\Phi=0$; far from the cross section the potential will take the form of Eq. (12). This classical problem, of interest for transmission lines, relates to the determination of the capacity per unit length C_l between two cylinders; with the electric field nearly radial at the outer circle one readily finds, using (12), $C_l \approx 2\pi\epsilon_0\alpha = 2\pi\epsilon_0/\ln(r_\infty/R_{\mathrm{eq}})$. This is indeed the capacity for an elliptical cross section when the particular R_{eq} given by (10) is used.[9]

Conformal mapping, expansions in circular harmonics, and image methods have been used to determine C_l in electrostatics, and thus $R_{\rm eq}$ here, for a variety of cross sections. For a regular polygon with n sides one has[9]

$$R_{\rm eq}=\frac{[\Gamma(1+1/n)]^2}{2\pi\Gamma(1+2/n)}p, \tag{13a}$$

where Γ is the gamma function; this leads to

$$R_{\rm eq}\approx p/7.11 \quad \text{for an equilateral triangle,} \tag{13b}$$

$$R_{\rm eq}\approx p/6.78 \quad \text{for a square.} \tag{13c}$$

For a general convex cross section one can solve for the potential in polar coordinates by expanding in circular harmonics.[10] For cross sections with a symmetry axis one has

$$\frac{\Phi(r,\theta)}{\Phi_P}=b_0\ln\frac{r}{r_\infty}+\sum_{m=1}^{\infty}b_m\frac{\cos m\theta}{r^m}\left(1-\frac{r^{2m}}{r_\infty^{2m}}\right),$$

having used $\Phi(r_\infty)=0$ and $\Phi(-\theta)=\Phi(\theta)$; for $r\gg p$ one recovers (12) with $\alpha=-b_0$. Setting $\Phi=\Phi_P$ at the cross section, where r/p will be some given function of θ, Fourier analysis would yield $R_{\rm eq}/p$ (and b_m/b_0p^m for $m\geqslant 1$). For a right-angle isosceles triangle one numerically finds

$$R_{\rm eq}\approx p/8.28. \tag{14}$$

We shall use these results in Sec. VI.

IV. SHAPE EFFECT FOR NONCONVEX CROSS SECTIONS

Failure of the OML law due to shape relates to the behavior of the potential field *near* the probe, ultimately dependent on the degree of cross section convexity. For the thin tape of Sec. III ($w_P=0$) we had found[2]

$$I/I_{\rm OML}(p)\approx 1-\gamma\alpha^2 \quad \text{for } R_{\rm eq}(=p/8)<R_{\rm max}. \tag{15}$$

The calculations in Appendix C of Ref. 2 give $\gamma(w_P=0)\approx 0.058$. Although a tape thus comes out not to be convex enough, its shape failure is quite weak; with α [given by (7)] logarithmically small for the bias of interest, the current in (15) lies less than 1% below the OML value.

The current reduction described by (15) can be understood by noticing that, for any point on the tape, trajectories that would hit it within some (very narrow) range of glancing angles are unpopulated: they would have come from other points on the tape, having kept close to it throughout.[8] This current reduction does not relate to size; it holds no matter how small $R_{\rm eq}$ or p. On the other hand, shape is here determinant; as w_P increases and an elliptical cross section evolves from thin tape to circle, the coefficient $\gamma(w_P)$ in Eq. (15) will finally vanish at some w_P, the OML current law certainly holding in the limit case of a small circle.

We now note that the reduction of current below the OML value for cross sections that are small can be substantial if they present definitely concave segments, as in the case of Fig. 2(a), a cross section made of two adjoining circles. Trajectories that hit a point on a concave segment would be unpopulated over a wide range of incoming angles. The

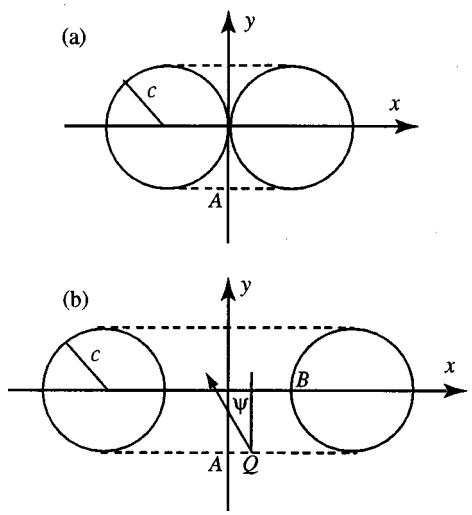

FIG. 2. Minimum-perimeter convex envelope (dashed and half-circle segments) for cross sections made of two circles of radius c each; (a) adjoining ($R_{\rm eq}\approx 1.57c$, $p_{\rm eq}\approx 10.28c$) and (b) at distance twice the diameter between centers ($R_{\rm eq}\approx 2.06c$, $p_{\rm eff}\approx 11.56c$).

OML law, nonetheless, may still be used to great accuracy if the actual full perimeter p, here $2\times 2\pi c$, is replaced in (1) by the perimeter $p_{\rm eq}$ of the minimum-perimeter (convex) envelope of the cross section, made of segments of the actual cross section and of straight segments, shown as dashed lines in Fig. 2(a). For the case of this figure, we would have $p_{\rm eq}=2\pi c+4c$. Regarding $R_{\rm eq}$, approximating the envelope as an ellipse and applying (10) would yield $R_{\rm eq}\approx \frac{1}{4}(c+2c)$. Actually, as recalled below, exact results for the capacity per unit length between the two-circle cylinder and a large, centered, circular cylinder yield $R_{\rm eq}=\pi c/2$,[10] and

$$6.55\,R_{\rm eq}\approx p_{\rm eq}\approx 0.82\,p. \tag{16}$$

To understand why Eq. (1) holds when p is replaced by $p_{\rm eq}$ note that (i) the value of $\sqrt{\Phi}(r)$ averaged over the minimum-perimeter envelope would be extremely close to the value $\sqrt{\Phi}_P$ in (1), as it will be shown below; (ii) all trajectories reaching the envelope from the faraway plasma would certainly hit the probe; and (iii) conditions in the vicinity of the *straight* (dashed) segments would be similar to conditions around a tape as far as convexity is concerned, resulting in current reduction that is fully negligible as in Eq. (15). Note that point (ii) would fail for any convex envelope of larger perimeter, while point (iii) would fail for a concave envelope lying between the actual cross section and its minimum-perimeter envelope (trajectories reaching such a concave envelope within a sensible range of incoming angles would be unpopulated). Introducing the value $p_{\rm eq}$ allows accurate use of the OML law for nonconvex cross sections, and proves helpful in discussing interference effects on collection.

To show how point (i) arises from the potential near a probe varying little in its vicinity, consider the Laplace solution for the potential between the two-circle cylinder of Figs. 2(a) or 2(b) and a centered cylinder of large radius r_∞ at vanishing potential,

$$\Phi(\bar{r})=\frac{-q}{2\pi\epsilon_0}\left[\ln|\bar{\rho}_l|+\ln\frac{|\bar{\rho}_l|}{|\bar{\rho}_l-\lambda_1 c\bar{i}|}+\sum_{k=1}^{\infty}\ln\frac{|\bar{\rho}_l-\lambda_{2k}c\bar{i}||\bar{\rho}_l-\lambda_{2k}c\bar{i}|}{|\bar{\rho}_l-\lambda_{2k-1}c\bar{i}||\bar{\rho}_l-\lambda_{2k+1}c\bar{i}|}\right]-\frac{q}{2\pi\epsilon_0}\left[\ln|\bar{\rho}_r|+\ln\frac{|\bar{\rho}_r|}{|\bar{\rho}_r+\lambda_1 c\bar{i}|}+\sum_{k=1}^{\infty}\ln\frac{|\bar{\rho}_r+\lambda_{2k}c\bar{i}||\bar{\rho}_r+\lambda_{2k}c\bar{i}|}{|\bar{\rho}_r+\lambda_{2k-1}c\bar{i}||\bar{\rho}_r+\lambda_{2k+1}c\bar{i}|}\right]+K, \tag{17}$$

$$\lambda_1\equiv\frac{c}{d},\quad \lambda_k=\frac{\lambda_1}{1-\lambda_1\lambda_{k-1}}\quad (k=2,3,...), \tag{18}$$

where d is the distance between centers, $\bar{i}$ is the unit vector for the x axis, and $\bar{\rho}_l\equiv\bar{r}+\bar{i}d/2$, $\bar{\rho}_r\equiv\bar{r}-\bar{i}d/2$. Since r_∞/c is very large, we described the potential outside the small cylinders in Figs. 2(a) and 2(b), by means of infinite sets of image line charges, with q the net charge per unit length in either cylinder. Starting with the q charges at the center lines, the left cylinder, say, becomes equipotential by introducing line images $-q$, a distance $\lambda_1 c$ to the right of its center, and $+q$, at the center (to keep the net charge).[10] Corresponding images for the right cylinder then require two new images in the left one: $+q$ and $-q$ at distances $\lambda_2 c$ and $\lambda_1 c$ from the center. In successive image iterations the distance $(\lambda_k-\lambda_{k-1})c$ between each couple of new line charges decreases, the series in (17) converging rapidly. Far away, Eq. (17) reads $\Phi\approx-(2q/2\pi\epsilon_0)\ln r+K$ to order c^2/r^2, condition $\Phi(r_\infty)=0$ thus requiring a constant $K=(2q/2\pi\epsilon_0)\ln r_\infty$.

For Fig. 2(a) we have $\lambda_1=1/2$, Eq. (18) then giving $\lambda_k=k/(k+1)$. At the origin in Fig. 2(a), Eq. (17) now reads

$$\Phi_P=\frac{-2q}{2\pi\epsilon_0}\left[\ln c+\ln 2+\ln\prod_{k=1}^{\infty}\left\{1-\frac{1}{(2k+1)^2}\right\}\right]+K=\frac{2q}{2\pi\epsilon_0}\ln\frac{2r_\infty}{\pi c},$$

yielding $C_l=2\pi\epsilon_0/\ln(r_\infty/R_{\rm eq})$, with $R_{\rm eq}=\pi c/2$ as already noted. At point A in Fig. 2(a) the two series in (17) converge very rapidly, yielding a potential $\Phi_A\approx(2q/2\pi\epsilon_0)\ln(r_\infty/1.71c)$. We then find $\sqrt{\Phi_A/\Phi_P}\approx1-0.04/\ln(r_\infty/R_{\rm eq})$. With $r_\infty\sim r_0$ as given in Sec. II, we have $\sqrt{\Phi_A/\Phi_P}\sim0.99$, the average value of $\sqrt{\Phi}(r)$ on the envelope differing from $\sqrt{\Phi}_P$ by a small fraction of 1%.

V. SHAPE EFFECT FOR DISJOINT CROSS SECTIONS

Consider the case of Fig. 2(b), with the centers of two disjoint circles at a distance four times the radius c. Here the mere concept of a minimum-perimeter envelope proves unsatisfactory, the current $I_{\rm OML}(p_{\rm eq})$, with $p_{\rm eq}=2\pi c+8c>2\times2\pi c$, exceeding the OML current for the full perimeter. This failure relates to condition (ii) in Sec. IV. For nonadjoining probes such as these, not all trajectories arriving at the dashed segments of the envelope from the far away plasma would hit the probe; some trajectories reach opposite dashed segments and escape.

Although the current density at the dashed segments may have the OML value, only some fraction f will correspond to trajectories reaching either circle. The OML law may still be used, however, if $p_{\rm eq}$ is replaced by some effective perimeter,

$$p_{\rm eq}\rightarrow p_{\rm eff}\equiv2\pi c+4\times2cf. \tag{19}$$

To determine the factor f consider electrons entering the envelope in Fig. 2(b) at a point Q between point A and the right circle $(0<x_Q<2c)$, and let ψ be the angle between the incoming velocity and the inward normal: trajectories within some range $\psi_r(x_Q)<\psi<\psi_I(x_Q)$ will miss both probes. The current reaching either probe from the segment to the right of point A is proportional to the integral[2]

$$\int_0^{2c}dx_Q\int_{\Delta\psi(x_Q)}\frac{\cos\psi\,d\psi}{2}\equiv f\times\int_0^{2c}dx_Q\int_{-\pi/2}^{\pi/2}\frac{\cos\psi\,d\psi}{2}=2cf, \tag{20}$$

where the ψ integration on the left excludes the range $\psi_r(x_Q)<\psi<\psi_I(x_Q)$.

Values ψ_r and ψ_I are easily determined for each point Q because trajectories are approximately straight inside the envelope. To justify this, use Eq. (17) with $d=4c$ to compute Φ_A and Φ_B in Fig. 2(b). The series converge very rapidly in both cases, yielding $\Phi_P=\Phi_B\approx(2q/2\pi\epsilon_0)\ln(r_\infty/R_{\rm eq})$ with $R_{\rm eq}\approx2.06c$, and $\Phi_A\approx(2q/2\pi\epsilon_0)\ln(r_\infty/2.46c)$. With $\sqrt{\Phi_A/\Phi_P}\approx1-0.09/\ln(r_\infty/R_{\rm eq})$, the average of $\sqrt{\Phi}(r)$ on the envelope would differ from $\sqrt{\Phi}_P$ by less than 1%. This results in a vector velocity that is nearly constant.

We then readily find $f\approx0.66$, leading to

$$5.61\,R_{\rm eq}\approx p_{\rm eff}\approx0.92\,p. \tag{21}$$

In Eq. (21) we used $R_{\rm eq}\approx2.06c$, too. Note that the simple calculation above would fail for distance between centers large, when trajectories between circles could not be approximated as straight. One could still determine f, however, by solving for trajectories in the Laplace near field.

VI. INTERFERENCE OF PARALLEL TETHERS

The interference of two or more parallel cylindrical probes as regards current collection shows mixed size and shape effects. Interference may be discussed on the basis of results for the special case of circular cross sections, as resumed in Eqs. (1)–(7), when extended to other cross sections by our introduction of equivalent radius $R_{\rm eq}$, and equivalent perimeter $p_{\rm eq}$ or effective perimeter $p_{\rm eff}$.

Consider, first, total current to two circular wires with full perimeter p. Equations (21) and (16) show that OML current ($\propto p_{\rm eff}$) at the position of Fig. 2(b) is 8% less than OML current collected by faraway wires, while current to wires at contact is 18% less. Shape interference is thus moderate at most. Note, however, that these results ignore any possible size effect, which proves to vary nonmonotonically with distance between wires. As this distance is reduced, the equivalent radius first increases from the value $R_{\rm eq}=c$ at

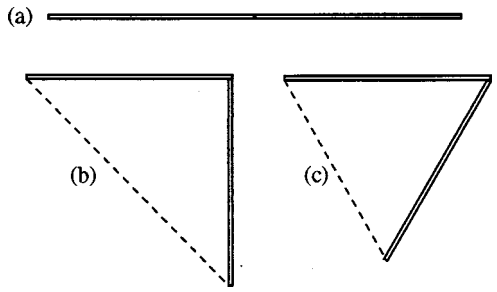

FIG. 3. Equivalent radius and perimeter for different orientations of two adjoining tapes of width l each: (a) $R_{eq}=0.5l$, $p_{eq}=4l$; (b) $R_{eq}\approx 0.41l$, $p_{eq}\approx 3.41l$; (c) $R_{eq}\approx 0.42l$, $p_{eq}=3l$.

large distances (corresponding to the single tether), reaches $R_{eq}\approx 2.06\,c$ in Fig. 2(b), and decreases to $R_{eq}\approx 1.57\,c$ at contact. Figure 1 suggests size effects will be small if c is less than R_{max}, whereas they can be large for $c>R_{max}$.

Consider now a large number N of circular wires regularly spaced in a straight row, with full perimeter $N\times 2\pi c$. When bringing the wires from large distances to contact ($p_{eq}\approx 4Nc$), shape effects decrease the current by a factor $2/\pi$, a reduction of 36%. Size effects could be dramatic: with $Nc\gg c$, the row of wires at contact would have $R_{eq}\approx p_{eq}/8\approx Nc/2\gg c$ (we approximated the row envelope as a thin tape). For N^2 wires regularly spaced in a square array, with full perimeter $N^2\times 2\pi c$, both shape and size effects can be dramatic. As next-neighbor distance goes from large to vanishing ($p_{eq}\approx 8Nc$), OML current decreases by a factor $4/\pi N$, while R_{eq} increases from c to a value $R_{eq}\approx p_{eq}/6.78\approx 1.18\,Nc$ [we approximated the envelope for the square array at contact as a square cross section, and used Eq. (13c)].

For thin tapes, relative orientation as well as distance affect interference. For two tapes of width l (full perimeter $4l$) brought from far away to contact, shape effects increase while any size effects roughly decrease, for the sequence of orientations shown in Figs. 3(a)–3(c) and Fig. 4(a). For Fig. 3(a) shape interference arises solely from the very small γ terms in Eq. (15), current decreasing by the factor $[1-\gamma\alpha^2(2l)]/[1-\gamma\alpha^2(l)]<1$; the effect is thus negligible. For Figs. 3(b), 3(c), and 4(a), ignoring the γ terms, p_{eq}, and thus OML current, is reduced by factors $(1+\sqrt{2})/2\sqrt{2}\approx 0.85$, 3/4, and 0.5, respectively. Regarding size effects, the inverse figure sequence, Figs. 4(a) and 3(c)–3(a), has R_{eq} increased from the value $l/4$, corresponding to the single tape, by factors 1, 1.69, 1.65, and 2, respectively; for Figs. 3(c) and 3(b) we used Eqs. (13b) and (14).

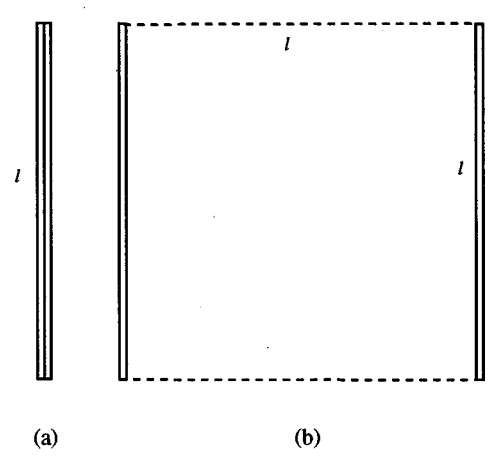

FIG. 4. Radius and perimeter of adjoining and close tapes at a particular orientation: (a) $R_{eq}=0.25l$, $p_{eq}=2l$; (b) $R_{eq}\approx 0.59l$, $p_{eff}\approx 3.17l$.

Concerning the effects of distance, consider Figs. 4(a) and 4(b). For Fig. 4(b), with $p_{eq}=p=4l$, we can proceed as in the case of Fig. 2(b). Writing $p_{eq}\rightarrow p_{eff}=2l+2l\times f$, we find $f=2-\sqrt{2}$ exactly. Also, using Eq. (13c) for a square, we have $R_{eq}\approx p_{eq}/6.78$, yielding

$$5.38\,R_{eq}\approx p_{eff}\approx 0.79p. \tag{22}$$

As the tapes approach each other keeping the disposition of Figs. 4(a) and 4(b), R_{eq} increases from the value $0.25l$ at large distances, reaches $R_{eq}\approx 0.59l$ in Fig. 4(b), and falls back to $0.25l$ for Fig. 4(a). The OML current for Fig. 4(b) is down by 21% from the OML current to far away tapes, while the current at contact is cut by one-half.

VII. DISCUSSION OF RESULTS

The current to a cylindrical probe of circular cross section had proved to be a product of two functions of perimeter p, and radius R, respectively, as given by Eqs. (1) and (2) and (2′) with R_{max} given in (4). Here we have extended results to arbitrary cross sections. For any convex cross section, certain solution of the two-dimensional Laplace equation served to determine an equivalent radius R_{eq} for use in the current law; for circle, square, equilateral triangle, and tape cross sections, the ratio p/R_{eq} takes values 2π, 6.78, 7.11, and 8, respectively. For R (or R_{eq}) $>R_{max}$ current drops below the OML value $I_{OML}(p)$ as a size effect related to behavior of the potential profile $\Phi(r)$ far from the probe.

For concave cross sections, p had to be replaced by a value $p_{eq}<p$, corresponding to the minimum-perimeter (convex) envelope of the cross section. The current drop below the OML value now relates to behavior of the potential near the probe. For the joint cross section of separate probes, p_{eq} was further replaced by a lower effective value $p_{eff}<p$, so as to take into account that not all trajectories entering the minimum-perimeter envelope reach either probe; for not too distant probes p_{eff} is easily determined because trajectories are then approximately straight within the envelope. Values for R_{eq}, p_{eq}, and p_{eff} for a variety of cross sections are shown in Figs. 2(a), 2(b), 3(a)–3(c), 4(a) and 4(b).

These results will allow to determine interference among parallel tethers under general conditions; this should prove useful in tether design. Interference between tapes is determined by both distance and relative orientation. For two tethers, maximum interference as regards shape occurs in Fig. 4(a), with OML current reduced by one-half from the joint current collected by the tapes if far from each other; note that a 50% reduction means that adding a second tape is useless as regards collection. For the tethers of Figs. 2(a), 2(b), 3(a)–3(c), and 4(b), OML current is reduced by factors 0.82, 0.92, 1, 0.85, 0.75, and 0.79, respectively, from the full current to distant tethers. For $N(\gg 1)$ round tethers in contact with each

other in a straight row, the reduction factor is 0.64; for N^2 ($\gg 1$) round tethers in contact in a square array, current is dramatically reduced by a factor $4\pi/N \ll 1$.

Size effects, if any, can be determined using Fig. 1. For round tethers, if distant from each other, the proper value for R_{eq} is the radius c of a single tether. For the two-tether of Figs. 2(a) and 2(b), R_{eq} is $1.57c$ and $2.06c$, respectively; for N tethers in contact with each other in a straight row and N^2 tethers in contact in a square array ($N \gg 1$), R_{eq} is $0.5Nc$ and $1.18Nc$, respectively. For distant tapes, R_{eq} is one-fourth of the width l of a single tape; for the two-tether of Figs. 3(a)–3(c) and 4(b) R_{eq} is greater by a factor 2, 1.65, 1.69, 1, and 2.36, respectively.

ACKNOWLEDGMENTS

The work by J.R.S. was supported by the Comisión Interministerial de Ciencia y Tecnología of Spain under Grant No. PB97-0574-C04-1. The work by R.D.E. was supported by NASA Grant No. NAG8-1605.

[1] J. R. Sanmartín, M. Martínez-Sánchez, and E. Ahedo, J. Propul. Power **9**, 353 (1993); R. D. Estes, J. R. Sanmartín, and M. Martínez-Sanchez, J. Spacecr. Rockets **37**, 197 (2000).
[2] J. R. Sanmartin and R. D. Estes, Phys. Plasmas **6**, 395 (1999).
[3] R. D. Estes and J. R. Sanmartín, Phys. Plasmas **7**, 4320 (2000).
[4] L. Johnson, R. D. Estes, E. Lorenzini, M. Martínez-Sánchez, and J. R. Sanmartín, J. Spacecr. Rockets **37**, 173 (2000); J. Ballance and L. Johnson, in *Space Technology and Applications International Forum-2001*, edited by M. S. El-Genk (American Institute of Physics, New York, 2001), p. 419.
[5] I. E. Vas, T. J. Kelly, and E. A. Scarl, J. Spacecr. Rockets **37**, 154 (2000); R. D. Estes, E. Lorenzini, J. R. Sanmartín, J. Peláez, M. Martínez-Sánchez, L. Johnson, and I. Vas, *ibid.* **37**, 205 (2000); J. H. Blumer, B. B. Donahue, and M. E. Bangham, in *Space Technology and Applications International Forum-2001*, edited by M. S. El-Genk (American Institute of Physics, New York, 2001), p. 445.
[6] R. L. Forward, R. P. Hoyt, and C. W. Uphoff, J. Spacecr. Rockets **37**, 187 (2000).
[7] J. R. Sanmartín, R. D. Estes, and E. Lorenzini, in *Space Technology and Applications International Forum-2001*, edited by M. S. El-Genk (American Institute of Physics, New York, 2001), p. 479.
[8] J. G. Laframboise and L. W. Parker, Phys. Fluids **16**, 629 (1973).
[9] W. R. Smythe and C. Yeh, in *American Institute of Physics Handbook*, edited by D. E. Gray (McGraw-Hill, New York, 1972), Sec. 5, p. 15.
[10] W. R. Smythe, *Static and Dynamic Electricity* (McGraw-Hill, New York, 1939), Chap. IV.